Critical dynamics of anisotropic antiferromagnets in an external field

Riya Nandi [*] and Uwe C. Täuber [†]

Department of Physics and Center for Soft Matter and Biological Physics, Virginia Tech, Blacksburg, Virginia 24061, USA

We numerically investigate the nonequilibrium critical dynamics in three-dimensional anisotropic antiferromagnets in the presence of an external magnetic field. The phase diagram of this system exhibits two critical lines that meet at a bicritical point. The nonconserved components of the staggered magnetization order parameter couple dynamically to the conserved component of the magnetization density along the direction of the external field. Employing a hybrid computational algorithm that combines reversible spin precession with relaxational Monte Carlo updates, we study the aging scaling dynamics for the model C critical line, identifying the critical initial slip, autocorrelation, and aging exponents for both the order parameter and the conserved field, thus also verifying the dynamic critical exponent. We further probe the model F critical line by investigating the system size dependence of the characteristic spin wave frequencies near criticality and measure the dynamic critical exponents for the order parameter including its aging scaling at the bicritical point.

I. INTRODUCTION

Classical anisotropic antiferromagnets governed by Heisenberg spin exchange in an external magnetic field exhibit a rich phase diagram with multiple thermodynamic ground states separated by continuous and discontinuous transition lines that meet at a multicritical point [1,2]. This paradigmatic model system describes various magnetic compounds including MnF_2 [3], $GdAlO_3$ [4], and $NiCl_2 \cdot 6H_2O$ [5] and, thus, has been extensively investigated theoretically as well as experimentally. Early renormalization-group [6], Monte Carlo simulation [7], and high-temperature expansion [8] studies have systematically explored its complex phase diagram and characterized the properties of the different ordered phases and determined the universality classes for its critical transition lines.

The anisotropy term along one of the crystal axes breaks the rotational symmetry of the Heisenberg antiferromagnet enforcing an antiparallel spin ordering along that axis in the low-temperature, low-field ground state, i.e., the Ising antiferromagnetic (AF) phase (cf. Fig. 1). As the external field strength is tuned up while the temperature is kept low, the ground-state switches, via a discontinuous (first-order) transition, to a spin-flop (SF) phase. At higher values of either temperature or magnetic field, the system becomes paramagnetic (PM). The phase transitions between the PM and the AF and SF states are both continuous (second order). While the associated static critical properties of the system are characterized solely by the symmetry and the dimensionality of the anisotropic Heisenberg Hamiltonian, the dynamics in the vicinity of the phase transitions driving it from the disordered phase to the ordered AF and SF phases, respectively, are

distinctly different and crucially depend on the microscopic, reversible dynamical couplings between the corresponding order parameters and the conserved magnetization components.

Indeed, the transition from the AF to the PM phase is described by the dynamic critical behavior of model C, while the SF-to-PM phase transition belongs to the dynamical universality class of model F; here we invoke the classification introduced by Halperin and Hohenberg in 1977 in their comprehensive early review of dynamic critical phenomena [9]. The presence of a nonordering field shifts the nonuniversal parameters of the system such as the critical temperature, but it does not change the nature of the critical point, i.e., the universal scaling exponents characterizing the critical power-law divergences remain unaltered. Yet an intriguing distinct physical scenario results in the vicinity of the *multicritical point*, where both critical lines as well as the discontinuous phase transition meet. At the multicritical point, all three different phases compete for the lowest free energy configuration; thus the system's symmetry at this special point is higher than in the adjacent parameter space. Hence, the dynamical properties in the vicinity of this point are expected to be characterized by new exponents which are distinct from those of the conjoining critical lines.

The nature of the multicritical point for anisotropic antiferromagnets subject to an external magnetic field (oriented along the z direction) has been somewhat controversial. This special point in parameter space is characterized by two coupled order parameter fields with $O(n_\perp) \oplus O(n_\parallel)$ symmetry; it displays long-range order both along the magnetic-field z axis and in the perpendicular xy plane. A series of papers by Folk, Holovatch, and Moser employed the renormalization group to investigate the static and dynamic critical behavior and the stability of the associated fixed points of the system [10–13]. They predicted the emergence of either bicritical behavior associated with a Heisenberg fixed point or tetracritical behavior, in turn associated with a biconical or a decoupled
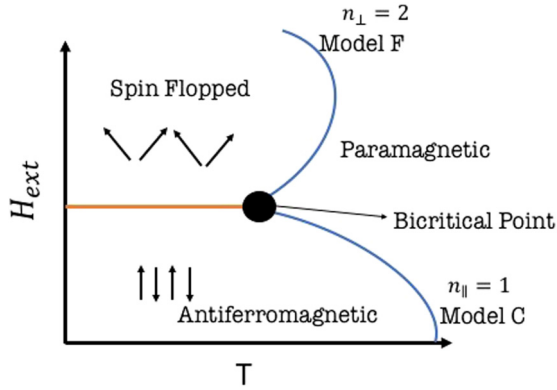
*[*]riya11@vt.edu

[†]tauber@vt.edu

FIG. 1. Schematic H_{ext}-T phase diagram of an anisotropic antiferromagnet in the presence of an external field showing two ordered phases separated by a first-order transition line. The antiferromagnetic and spin-flopped ordered phases are separated from the disordered paramagnetic phase by lines of continuous phase transitions that meet at a bicritical point.

renormalization-group fixed point. An analysis to higher order resulted in the tetracritical point with a biconical phase to represent the stable fixed point [14]. A recent six-loop perturbative dimensional ϵ expansion of the three-dimensional n-vector model has shown that for $n = 3$, the obtained critical exponents are very close to the Heisenberg fixed point values even though that is not the stable fixed point in the asymptotic infrared limit [15]. Thus, the observed critical behavior in experiments and simulations may be indistinguishable from the isotropic Heisenberg fixed point scaling. This has indeed been observed to be true in a series of detailed Monte Carlo simulations analyzing order parameter susceptibilities, the Binder cumulant, and associated probability distributions, which reported that the nature of the multicritical point is in fact *bicritical* with Heisenberg symmetry [16,17].

While the static critical behavior and stationary critical dynamics of this system have been investigated comprehensively in the literature, we are not aware of previous computational work addressing the nonequilibrium critical relaxation of the anisotropic Heisenberg antiferromagnet in an external magnetic field either near the continuous phase transition line or at the multicritical point. To this end, the system is initially prepared in a disordered configuration and then quenched precisely to its critical point such that the dynamics algebraically slowly evolves towards the asymptotic stationary state. During this early nonequilibrium relaxation time window, the system retains the memory of its initial state and, thus, manifests broken time translation invariance. By studying the ensuing aging scaling behavior of two-time quantities at these early times, one may fully characterize the dynamics near the distinct critical points and the corresponding universality classes [18,19].

In this work, we utilize a hybrid simulation method combining relaxational Monte Carlo kinetics and reversible spin precession processes [20] to explore the aging scaling behavior of the AF-to-PM model C critical line and in the vicinity of the multicritical point. We measure the critical aging scaling, autocorrelation decay, and initial slip exponents for the model C universality class and determine the

associated dynamic critical exponent. We also investigate the nonequilibrium dynamics of the conserved magnetization component. Furthermore, we utilize Fourier spectral analysis for the spin-wave excitations in the xy plane in the SF ordered phase to verify the dynamic critical exponent for the SF-to-PM model F critical line. Finally, we investigate the critical order parameter dynamics at the bicritical point.

II. MODEL AND SIMULATION METHOD

The Hamiltonian of a three-dimensional antiferromagnet with anisotropic Heisenberg exchange interactions in an external magnetic field is given by

$$\mathcal{H} = J \sum_{\langle ij \rangle}^{N} \left[\Delta \left(S_i^x S_j^x + S_i^y S_j^y \right) + S_i^z S_j^z \right] - H_{ext} \sum_{i=0}^{N} S_i^z, \quad (1)$$

where S_x^i, S_y^i, and S_z^i represent the components of the three-dimensional spin vector $\vec{S}^i$ at the ith site of a simple cubic lattice of linear extension L with total spin number $N = L^3$. The magnitude of the spins is fixed to unit magnitude, $S_x^{i2} + S_y^{i2} + S_z^{i2} = 1$. $J > 0$ denotes the antiferromagnetic exchange interaction along the z axis between nearest-neighbor spin pairs $\langle ij \rangle$; we set $J = +1$, i.e., measure temperature in units of J/k_B and the external field in units of J. The uniaxial anisotropy $0 < \Delta < 1$ imposes an "easy" z axis such that the spins would order antiparallel along this direction in the absence of an external field [16]; we choose $\Delta = 0.8$. The presence of this anisotropy explicitly breaks the $O(3)$ rotational symmetry of the Hamiltonian in spin space and splits it into two subspaces of dimensions $n_\parallel = 1$ and $n_\perp = 2$. Thus its static critical properties are governed by the universality class with $O(1) \oplus O(2)$ symmetry with the associated Fisher exponent $\eta \approx 0.04$ [10].

Applying an external magnetic field $H_{ext} \neq 0$ along the z axis forces the uniaxially aligned spins to flop over into the xy plane beyond some critical field strength H_{ext}^c. Thus, at a low temperature T and external field H_{ext}, i.e., in the AF phase, the z component of the staggered magnetization

$$\phi_\parallel = \sum_{i,j,k=0}^{L} (-1)^p S_{i,j,k}^z \quad (2)$$

represents the nonconserved order parameter for the system; here the indices (i, j, k) denote the three spatial directions, and $p = i + j + k$ ensures that the sum extends over the differences between every alternate spin in the lattice. Upon increasing H_{ext}, the value of $\phi_\parallel$ is diminished, and instead the staggered magnetization components in the xy plane perpendicular to the applied field become appreciable. Thus in the SF phase, an appropriate, also nonconserved, order parameter is a two-component vector $\vec{\phi}_\perp = (\phi_x, \phi_y)$ with magnitude

$$\phi_\perp = \sqrt{\left(\sum_{i,j,k=0}^{L} (-1)^p S_{i,j,k}^x \right)^2 + \left(\sum_{i,j,k=0}^{L} (-1)^p S_{i,j,k}^y \right)^2}. \quad (3)$$

It is important to note that Hamiltonian (1) conserves the z component of the total magnetization

$$M_z = \sum_{i,j,k=0}^{N} S_{i,j,k}^z \qquad (4)$$

under the dynamics, $\{\mathcal{H}, M_z\} = 0$; here the Poisson bracket constitutes the classical counterpart of the quantum-mechanical commutation relation between the spin angular momentum and the Hamiltonian. The dynamical mode couplings between conserved magnetization fluctuations and the order parameter components decisively influence the antiferromagnet's critical dynamics [9,19,21,22]. Indeed, in addition to the irreversible, relaxational terms arising from the static couplings in the Hamiltonian, one must account for the *reversible* kinetics caused by the underlying microscopic dynamics between the order parameter and any conserved modes. At zero temperature, the microscopic equations of motion obeyed by each spin variable are $dS_i^\alpha(t)/dt = \{\mathcal{H}, S_i^\alpha(t)\}$, where the spin vector components satisfy the standard angular momentum Poisson brackets $\{S_i^\alpha, S_j^\beta\} = \sum_\gamma \epsilon^{\alpha\beta\gamma} S_i^\gamma \delta_{ij}$ with the fully antisymmetric unit tensor $\epsilon^{\alpha\beta\gamma} = \pm 1$.

In the $n_\parallel = 1$ subspace $\{M_z, \phi_\parallel\} = 0$; thus there is no reversible coupling term. However, in the $n_\perp = 2$ subspace, the nonconserved vector order parameter $\vec{\phi}_\perp$ couples reversibly to the conserved magnetization, (4),

$$\{M_z, \phi_\alpha\} = \epsilon_{\alpha\beta z}\phi_\beta, \qquad (5)$$

where $\alpha, \beta \in \{x, y\}$. This nonvanishing mode coupling gives rise to the deterministic equations of motion of the microscopic spin components at $T = 0$ [21,23]

$$\frac{d\vec{S}_i(t)}{dt} = \vec{S}_i(t) \times \frac{\partial \mathcal{H}}{\partial \vec{S}_i(t)}, \qquad (6)$$

which describe precession of the unit spin vector in the local effective field.

To simulate the dynamics of this system at finite temperature, one needs to implement relaxation terms as well as the reversible microscopic equations of motion. For convenience, we work with the two angular degrees of freedom ϑ and φ that are related to the unit vector spin components through $(S_x, S_y, S_z) = (\sin\vartheta\cos\varphi, \sin\vartheta\sin\varphi, \cos\vartheta)$. To respect the underlying conservation property, the azimuthal angles ϑ are updated by means of Kawasaki Monte Carlo kinetics where two randomly picked neighboring spins exchange their ϑ values following the standard Metropolis rules [24]. In contrast, the polar angles φ are evolved using Glauber dynamics where the spin component at the selected lattice site is subjected to a finite rotation with again Metropolis updates [25]. These Monte Carlo update steps of the spin configurations are alternated with a fourth-order Runge-Kutta integration of the equations of motion, (6) [20]. For our simulation, the integration was performed in parallel on all spins over discrete time increments $\Delta t = 0.01/J$, with each integration step separated by 10 Monte Carlo sweeps over the entire lattice. We determined this combination to be optimal in maintaining the conservation laws within the truncation error bounds of the numerical integration scheme.

III. MODEL C DYNAMICAL SCALING

The dynamical universality class conventionally labeled as model C describes the pure relaxation dynamics of a nonconserved n-component critical order parameter field, coupled to a conserved density [9,19,22,26]. In the present study, the low-temperature, low-field ground state is an Ising antiferromagnet; hence $n = 1$, with the z component of the magnetization density constituting the conserved scalar field m. A two-loop renormalization group calculation demonstrated that the scalar model C ($n = 1$) is governed by a strong-scaling fixed point with both the order parameter relaxation and the conserved density diffusion scaling with the same anomalous exponent α/ν [27]. This results in the *dynamic critical exponent* $z_z = z_m = 2 + \alpha/\nu \approx 2.185$; here $\nu \approx 0.72$ [28,29] describes the algebraic divergence of the correlation length $\xi \sim |\tau|^{-\nu}$ ($\tau \sim T - T_c$), and α is the specific heat critical exponent, $C \sim |\tau|^{-\alpha}$, which can be obtained from the hyperscaling relation $\alpha = 2 - d\nu$ in d dimensions.

The nonequilibrium relaxation of model C was investigated by Oerding and Janssen using the dynamic renormalization-group approach [30]. Following a critical quench, the two-time order parameter correlation function relating two space-time points at distance r and times $s < t$ satisfies the scaling law

$$C(t, s, r, \tau) = r^{-(d-2+\eta)} (t/s)^{\theta-1} \hat{C}(r/\xi, t/\xi^z), \qquad (7)$$

where θ is the *initial slip exponent*, representing a new independent universal exponent for purely dissipative systems with a nonconserved order parameter [31]. It also describes the power-law growth of the order parameter in the early-time universal regime which sets in right after the microscopic time during the nonequilibrium relaxation process. At the critical temperature $T = T_c$ ($\tau = 0$), the two-time autocorrelation function ($r = 0$) assumes the simple-aging scaling form [18],

$$C(t, s) \sim s^{-b} (t/s)^{-\lambda/z}, \qquad (8)$$

with the static and dynamic exponents related to the *scaling collapse exponent* b via

$$b = (d - 2 + \eta)/z \qquad (9)$$

and to the *autocorrelation exponent* λ according to

$$\lambda = d - 2 + \eta + z(1 - \theta) = z(1 + b - \theta). \qquad (10)$$

For model C with $n = 1$, a second-order perturbative renormalization calculation predicts $\theta \approx 0.27$ in three dimensions, if one boldly extrapolates the dimensional expansion in $\epsilon = 4 - \epsilon$ to $\epsilon = 1$ [30].

To numerically study the critical relaxation and the aging scaling regime we initialized the system in a disordered spin orientation configuration corresponding to a very high temperature and subsequently performed critical quenches to a point ($T_c = 1.5$, $H_{\text{ext}}^c = 3.0$) on the model C critical line. As shown in Fig. 2(a), we obtain an aging scaling window for waiting times $s = 120 \ldots 200$ simulation time steps. The inset demonstrates that time translation invariance is broken, as the two-time correlation function for the order parameter $C_{\text{SM}}^z(t, s)$ is not simply a function of the time difference $t - s$, as it would be in the stationary limit, but evolves differently for the distinct waiting times s in this temporal window. By
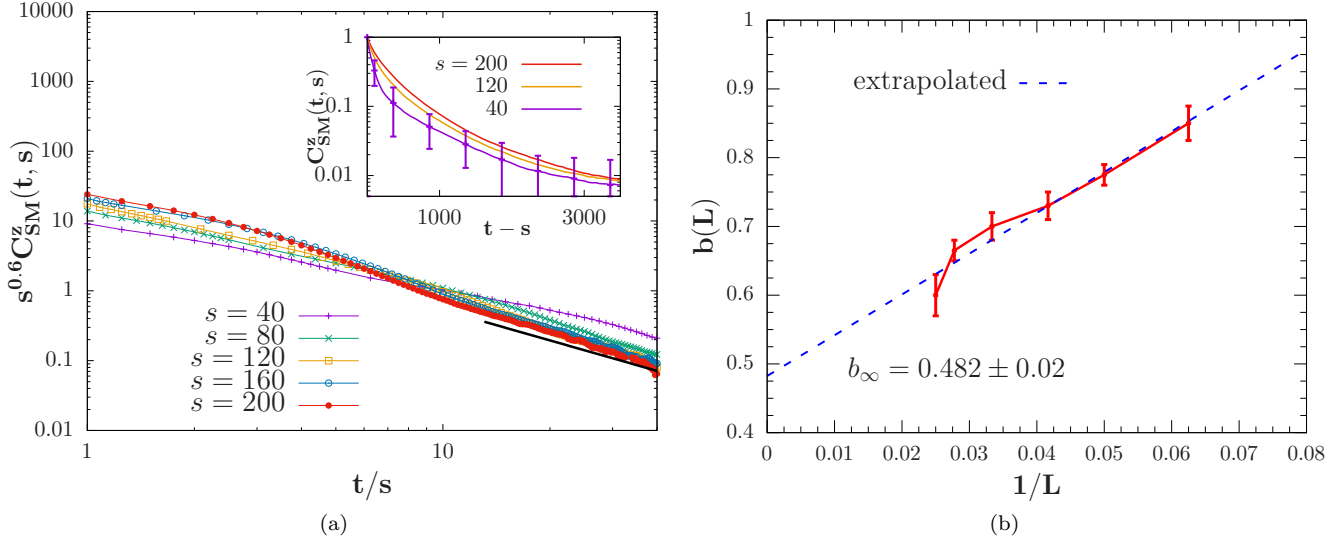
FIG. 2. (a) Aging scaling plots for the two-time spin autocorrelation function $C^z_{SM}(t, s)$ of the Ising antiferromagnetic order parameter on a simple cubic lattice of linear system size $L = 40$ with periodic boundary conditions. The system is quenched from an initially disordered configuration to the critical point at $T_c = 1.5$, $H^c_{ext} = 3.0$. Double-logarithmic rescaled graphs for different waiting times s collapse with the scaling exponent $b = 0.6$. Inset: Autocorrelation plots as a function of $t - s$ (in simulation time steps) for $s = 200$, 120, and 40 (top to bottom), demonstrating broken time translation invariance. Statistical errors are indicated in the graph for the shortest waiting time, $s = 40$. (b) Finite-size extrapolation analysis for the aging exponent $b(L)$ plotted vs $1/L$ for six system sizes, $L = 16 \ldots 40$. A linear extrapolation to the infinite system size limit $L \to \infty$ yields $b_\infty = 0.482 \pm 0.02$.

collapsing the data for $C^z_{SM}(t, s)$ for several waiting times s plotted as a function of the time ratio t/s in accordance with Eq. (8), one can obtain the collapse exponent b for which we find $b \approx 0.6$ for linear system extension $L = 40$. The data collapse is noticeably improved for both later waiting times s and longer observation times t. This is expected since the simple-aging scaling form, (8), is supposed to hold only for sufficiently large $t \gg s$ and s.

However, in our finite simulation domain, data for large times are inevitably hindered by finite-size effects. Thus, in order to better estimate the asymptotic collapse exponent, we perform a systematic finite-size extrapolation analysis by plotting b vs $1/L$ for system sizes $L = 16$, 20, 24, 30, 36, and 40 [cf. Fig. 2(b)]. Linear extrapolation to an infinite system size $L \to \infty$ leads to $b_\infty = 0.482 \pm 0.02$. We then obtain from Eq. (9) the dynamic exponent for the order parameter in model C in $d = 3$ dimensions, $z_z = (1 + \eta)/b = 2.158 \pm 0.09$. This result agrees well within our errors with the theoretically predicted value $z_z \approx 2.185$. The autocorrelation exponent λ/z_z can be extracted from the power-law tails of $C^z_{SM}(t, s)$, apparent in double-logarithmic plots vs t/s for times $t \gg s$. Figure 3 displays the data for five system sizes, from which we obtain the mean value $\langle\lambda/z_z\rangle = 1.342 \pm 0.06$. Using Eq. (10), one may obtain the initial slip exponent $\theta = 0.14 \pm 0.08$. This value shows a trend similar to that of the theoretical prediction but, unsurprisingly, differs in magnitude by a factor of about 2 from the naive extrapolation of the second-order results of the perturbative ϵ expansion about the mean-field value $\theta = 0$.

We further explore the nonequilibrium dynamics of the conserved magnetization component M_z which is reversibly coupled to the ordered parameter. This noncritical conserved field undergoes diffusive relaxation with correlations $C_m(\vec{q}, \omega) \sim q^{-2}\hat{C}(\omega/q^z)$ or, equivalently, $C_m(\vec{r}, t) \sim$

$r^{-(d-2)}\tilde{C}(r/t^z)$. The asymptotic long-time scaling form for the temporal magnetization correlation function at the critical temperature thus becomes

$$C_m(t) \sim t^{-(d-2)/z}. \tag{11}$$

In the data depicted in Fig. 4(a), we discern an intermediate power-law region in the decay of the spin autocorrelation function before the graphs fall off exponentially due to finite-size effects. As expected, this algebraic regime becomes more
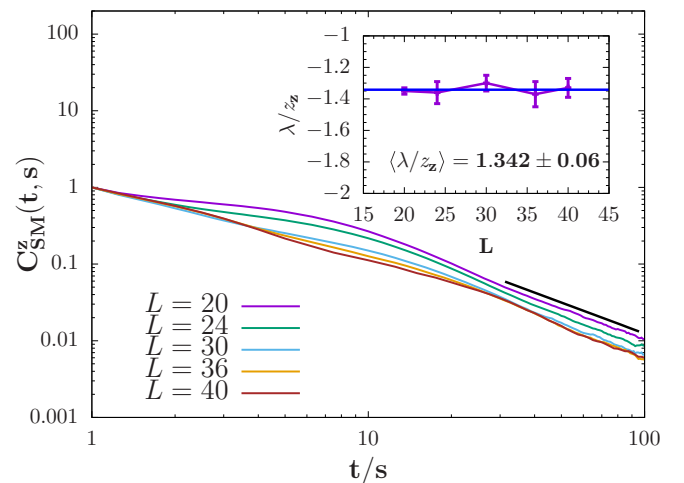

FIG. 3. Double-logarithmic plots of the two-time staggered magnetization autocorrelation function vs t/s for different linear system sizes $L = 20, \ldots, 40$ (top to bottom) taken at an early waiting time, $s = 40$, exhibit power-law decays in the long-time limit $t \gg s$. The mean value of the autocorrelation exponent is determined to be $\langle\lambda/z_z\rangle = 1.342 \pm 0.06$.
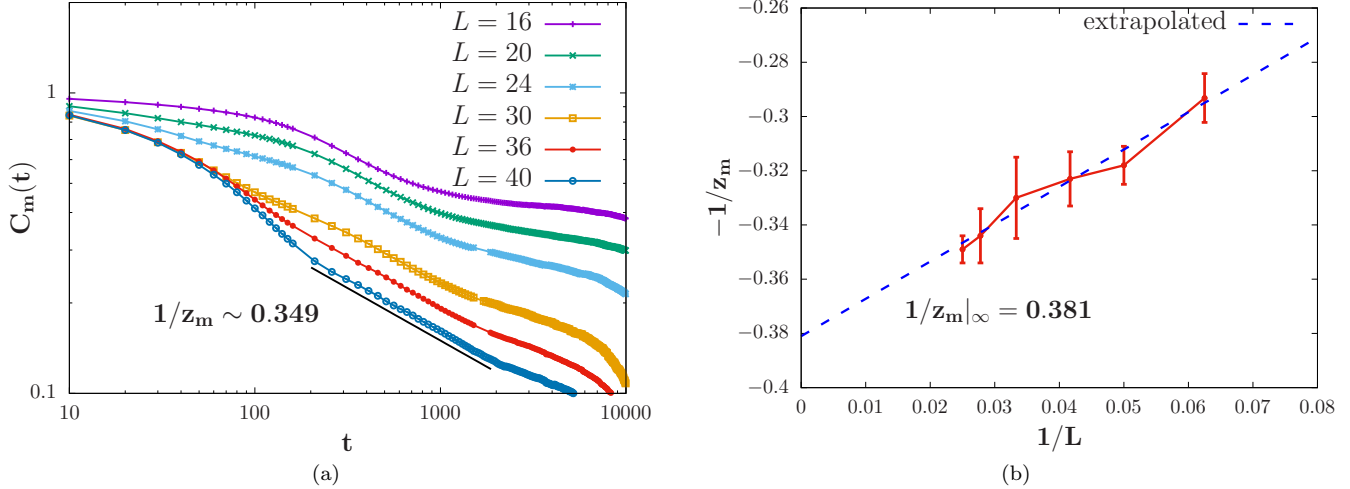
FIG. 4. (a) Double-logarithmic plots of the autocorrelation function for the conserved magnetization component M_z vs time t for different linear system sizes L display an intermediate regime governed by algebraic decay. The system was quenched to the critical point at $T_c = 1.5$, $H_{ext}^c = 3.0$. (b) Finite-size extrapolation analysis for the decay exponent plotted vs $1/L$ for six system sizes, $L = 16 \ldots 40$. A linear extrapolation to the infinite system size limit $L \to \infty$ yields $1/z_m = 0.381$.

prominent upon increasing the linear system size L. We again perform a systematic finite-size extrapolation to obtain the asymptotic value of the decay exponent, find $(1/z_m)_\infty \approx 0.381$, and thus infer $z_m \approx 2.62 \pm 0.01$. This value, however, differs from the order parameter dynamic exponent $z_z \approx 2.148 \pm 0.1$, indicating that likely the time-scale ratio between the staggered magnetization relaxation and the magnetization diffusion still has not reached its asymptotic fixed point, and the strong dynamic scaling hypothesis cannot be validated. In this context, we direct the readers to previous work by Koch and Dohm discussing the effect of finite system size on the relaxation and diffusion time scales of model C [32].

One can also obtain the aging scaling data from the two-time autocorrelation function for the conserved magnetization (cf. Fig. 5). We note, though, that for long waiting times we observe another power-law region at later times which is distinctly different from the previously obtained algebraic decay in the intermediate relaxation regime of the single-time autocorrelation function. It is at these later times that the rescaled plots for different waiting times collapse with an exponent $b_m \sim -0.3$ and a decay exponent equal to 0.239 ± 0.01. Earlier analyses of conserved spin systems have predicted two regimes with different power laws, with a new length scale governing the crossover between both algebraic regimes [33,34]. Ultimately in the long-time limit, however, the decay of the autocorrelations is determined by only one length scale, independent of the waiting time s. In a similar vein, the noncritical conserved magnetization here displays the signature of two distinct scaling regimes. Yet unlike in the conserved spin systems, we observe an early relaxation regime with a faster power-law decay, prominent in the single-time autocorrelation plots in Fig. 4, which subsequently crosses over to a slower algebraic decay until ultimately finite-size effects dominate. Moreover, the negative value of the exponent b_m suggests the presence of long-lived metastable states. The precise nature of the crossover scaling for the conserved magnetization in our system thus remains open for future investigation.

IV. MODEL F DYNAMICAL SCALING

The continuous phase transition between the spin-flop and the paramagnetic phases is described by the dynamic universality class model F [9,22]. Also known as the "asymmetric planar spin model" [35], this universality class describes the critical dynamics of a two-component vector order parameter coupled reversibly to a conserved scalar density in the presence of an external Z_2 symmetry-breaking field. The only other known and prominent physical system described by model F is the normal fluid–to–superfluid transition in ^{4}He [36]. In anisotropic antiferromagnets, the nonconserved components of the planar staggered magnetization ϕ_x and ϕ_y
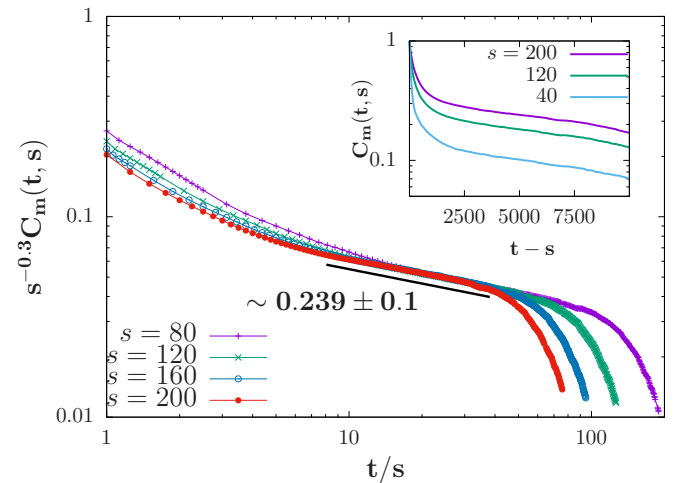

FIG. 5. Aging scaling plots for the two-time autocorrelation function $C_m(t, s)$ of the conserved magnetization for linear system size $L = 40$. Double-logarithmic rescaled plots for different waiting times s collapse with exponent $b_m \approx -0.3$ and decay exponent $\approx 0.239 \pm 0.1$. Inset: Autocorrelation plots as a function of $t - s$ for $s = 200$, 120, and 40 (top to bottom), demonstrating broken time translation invariance.
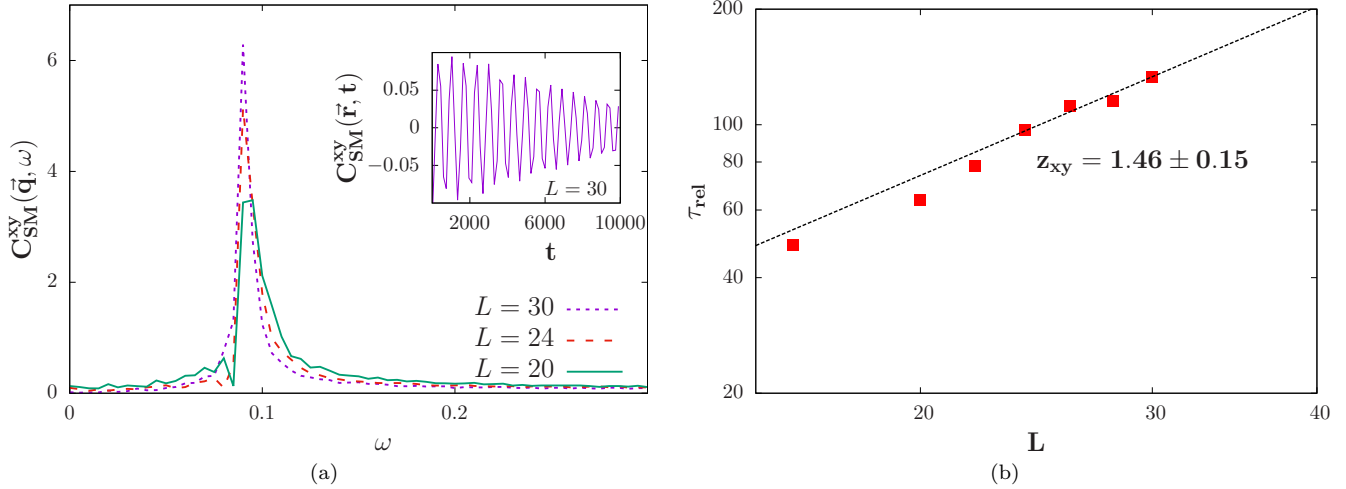
FIG. 6. (a) Fourier spectrum of the staggered magnetization correlation function in the xy plane for different linear system sizes, $L = 20$, 24, and 30, for a nonzero wave vector $\vec{q}$ vs the frequency ω. Inset: Propagating spin waves in the spin-spin correlation function with spatial separation $\vec{r}$ as a function of time. (b) Double-logarithmic plot of the relaxation time τ_{rel} vs linear system sizes $L = 16 \ldots 32$. Fitting the data for large $L > 20$ yields the dynamic critical exponent $z = 1.46 \pm 0.15$.

couple reversibly through the nonvanishing Poisson brackets to the conserved magnetization component M_z, resulting in the precession motion, (5), of the spin vectors around a local field produced by their exchange interaction with their nearest neighbors and the external field.

One may view the conserved magnetization components acting as the infinitesimal rotation generators for the order parameter components, resulting in propagating spin waves in the ordered phase [19,37]. The spin-wave damping Γ_c decreases as the critical temperature is approached, with the associated relaxation time $\tau_{\text{rel}} = 1/\Gamma_c$ diverging at T_c. Hence procuring the aging scaling data by probing the conventional

two-time correlations turns out not to be a viable approach at the model F critical line. Moreover, owing to the reversible mode couplings between the conserved magnetization and the nonconserved order parameter components, the initial slip exponent θ and hence the autocorrelation exponent λ are expected to be nonuniversal in this case; specifically, these exponents should depend on the initial distribution of the magnitudes of the conserved modes [20,38].

However, one can extract the dynamic exponent from the temporal evolution of the stationary correlation function in the vicinity of the critical parameters in the ordered phase. Near the critical temperature, the spin-wave oscillations have
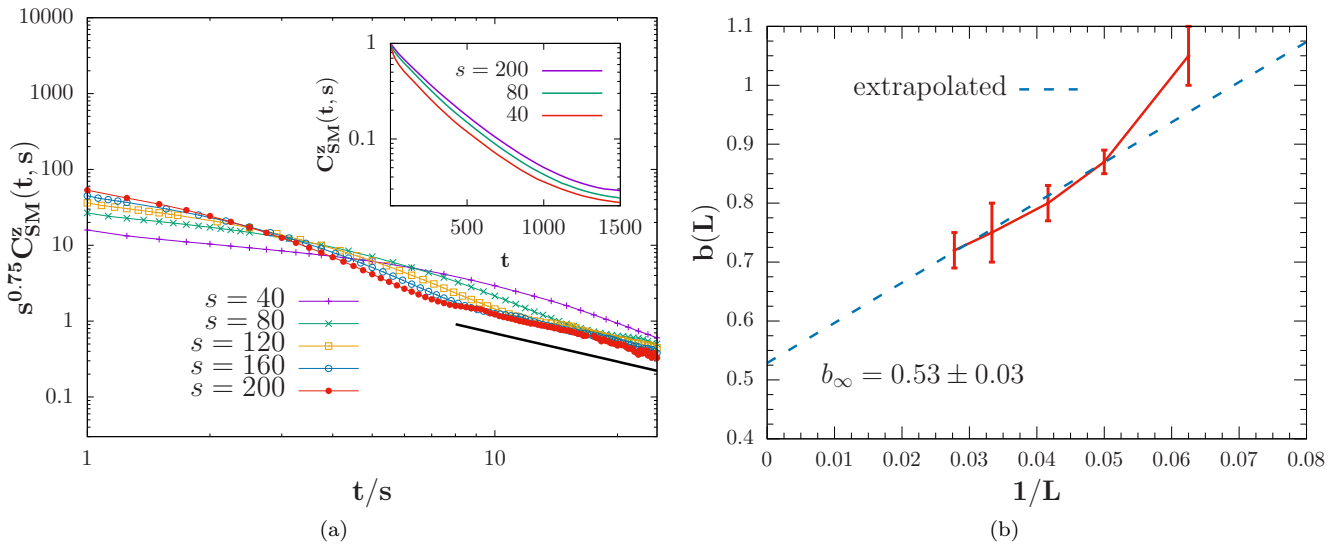

FIG. 7. (a) Aging scaling plots for the two-time spin autocorrelation function $C_{\text{SM}}^z(t, s)$ of the Ising antiferromagnetic order parameter on a simple cubic lattice of linear system size $L = 30$ with periodic boundary conditions. The system is quenched from an initially disordered configuration to the bicritical point at $T_c = 1.025$, $H_{\text{ext}}^c = 3.825$. Double-logarithmic rescaled graphs for different waiting times s collapse with the scaling exponent $b \approx 0.75$. Inset: Autocorrelation plots as a function of $t - s$ for $s = 200$, 80, and 40 (top to bottom), demonstrating broken time translation invariance. (b) Finite-size extrapolation analysis for the aging exponent b plotted vs $1/L$ for five linear system sizes, $L = 16 \ldots 36$. A linear extrapolation using the data from the four largest systems to the infinite system size limit $L \to \infty$ yields $b_\infty = 0.53 \pm 0.03$.

an exponentially decreasing amplitude $\sim e^{-\Gamma_c t} \sim e^{-t/\tau_{\rm rel}}$. In a finite system near T_c, the stationary relaxation time diverges with the linear system size, with the dynamic critical exponent z characterizing its *critical slowing-down*: $\tau_{\rm rel} \sim L^z$. We have obtained the relaxation time via measuring the half-peak width Γ_c of the Fourier transform of the spin-spin correlation function [39], $C_{\rm SM}^{xy}(\vec{q}, \omega) = \int C_{\rm SM}^{xy}(\vec{r}, t) e^{i\omega t} dt$ [see Fig. 6(a)]. The asymptotic value of the dynamic exponent for model F is known exactly from the dynamic renormalization group, $z_{xy} = d/2$ in $d \leqslant 4$ dimensions [35,40]. From our relaxation time data as a function of the linear system size, we find that for the five largest L values the best-fit line gives $z_{xy} \approx 1.46$, within our error bars, in agreement with the theoretical prediction 1.5 [cf. Fig. 6(b)]. As one would expect, with larger system sizes z_{xy} tends towards the asymptotic value.

V. BICRITICAL DYNAMICAL SCALING

The two continuous phase transition lines described by models C and F meet at a *bicritical point* which is described by a different dynamical universality class. In their field-theoretical analysis, Folk, Holovatch, and Moser found that irrespective of whether the static behavior of the system is described by the Heisenberg or the biconical renormalization-group fixed point, the parallel and perpendicular order parameter components scale similarly in time, with dynamic critical exponents $z_z \sim z_{xy} \approx 2.003$ and $z_m \approx 1.542$ in the asymptotic limit [13]. However, strong nonasymptotic effects originating from the mode coupling terms in the vicinity of the bicritical point lead to very different crossover dynamical exponents which exhibit weak dynamical scaling.

Similarly to the model C analysis, we obtain a dynamic aging scaling window for waiting times $s = 80 \ldots 200$ for the easy-axis scalar order parameter at the bicritical point. Figure 7 depicts the scaling collapse of the two-time autocorrelation plots for different waiting times for a system with linear size $L = 30$ with aging exponent $b \approx 0.75$. A subsequent system size extrapolation yields the asymptotic value $b_{\infty} = 0.53 \pm 0.03$. Using Eq. (9), one can then infer the dynamic critical exponent $z_z = 1.962 \pm 0.15$, which is in agreement with the theoretical prediction within our error bars. From the mean value of $\langle \lambda/z_z \rangle = 1.265 \pm 0.03$ over five system sizes (cf. Fig. 8), we also obtain the bicritical initial slip exponent $\theta = 0.265 \pm 0.05$ for the staggered magnetization along the z axis.

VI. CONCLUSION

We have utilized a hybrid numerical method that incorporates reversible spin precession dynamics through a deterministic integration scheme with relaxational Monte Carlo kinetics to investigate both the stationary critical dynamics and the nonequilibrium critical relaxation in three-dimensional anisotropic antiferromagnets in an external magnetic field. From the aging scaling data of the order parameter spin autocorrelation function at the model C critical line, we obtained the aging and autocorrelation exponents. A systematic finite-size extrapolation analysis allowed for the extraction of the asymptotic value of the aging collapse
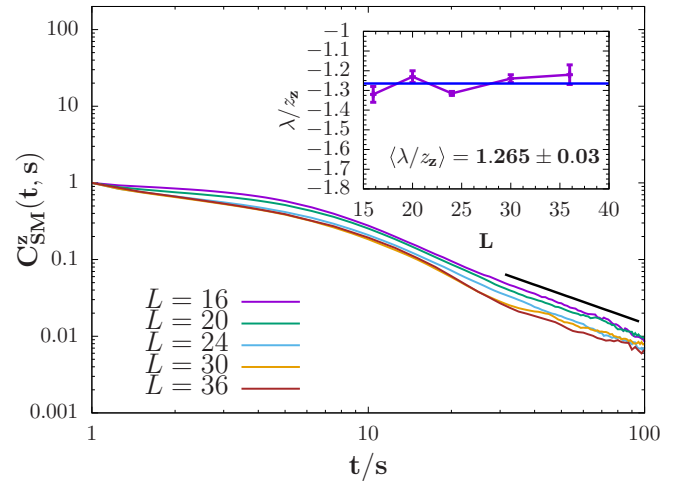

FIG. 8. Double-logarithmic plots of the two-time staggered magnetization autocorrelation function vs t/s for different linear system sizes, $L = 16, \ldots, 36$ (top to bottom), taken at an early waiting time, $s = 40$, exhibit power-law decays in the long-time limit $t \gg s$. The mean value of the autocorrelation exponent is determined to be $\langle \lambda/z_z \rangle = 1.265 \pm 0.03$.

exponent $b \approx 0.482$, which leads to the dynamic exponent $z_z \approx 2.148$. This is in very good agreement with the theoretical prediction. Further, we report the value of the initial slip exponent $\theta \approx 0.14$. Additionally, we extract the dynamic exponent for the conserved magnetization $z_m \approx 2.62$ and observe two distinct time scales in the decay of its two-time spin autocorrelation function.

In the vicinity of the model F critical line, the presence of spin waves hindered the aging scaling analysis. However, from the Fourier transform analysis of the spin waves we obtained the critical relaxation times that increase algebraically with the system size, with the dynamic critical exponent $z_{xy} \approx 1.46$, which agrees with the theoretical value $z_{xy} = 3/2$ within our systematic and statistical errors. Finally, we performed an aging scaling analysis for the scalar order parameter component along the direction of the external field at the bicritical point. We thus verified that the dynamic exponent at this point, $z_z \approx 1.962$, is different from the corresponding values at both the model C and the model F critical lines, contrasting with the nature of the dynamical universality class at the bicritical point.

[1] J. M. Kosterlitz, D. R. Nelson, and M. E. Fisher, Phys. Rev. B **13**, 412 (1976).

[2] K. S. Liu and M. E. Fisher, J. Low Temp. Phys. **10**, 655 (1973).

[3] Y. Shapira and S. Foner, Phys. Rev. B **1**, 3083 (1970).

[4] H. Rohrer and C. Gerber, Phys. Rev. Lett. **38**, 909 (1977).

[5] N. F. Oliveira Jr., A. Paduan Filho, S. R. Salinas, and C. C. Becerra, Phys. Rev. B **18**, 6165 (1978).

[6] M. E. Fisher and D. R. Nelson, Phys. Rev. Lett. **32**, 1350 (1974).

[7] D. P. Landau and K. Binder, Phys. Rev. B **17**, 2328 (1978).

[8] O. G. Mouritsen, E. Kjaersgaard Hansen, and S. J. Knak Jensen, Phys. Rev. B **22**, 3256 (1980).

[9] P. C. Hohenberg and B. I. Halperin, Rev. Mod. Phys. **49**, 435 (1977).

[10] R. Folk, Y. Holovatch, and G. Moser, Phys. Rev. E **78**, 041124 (2008).

[11] R. Folk, Y. Holovatch, and G. Moser, Phys. Rev. E **78**, 041125 (2008).

[12] R. Folk, Y. Holovatch, and G. Moser, Phys. Rev. E **79**, 031109 (2009).

[13] R. Folk, Y. Holovatch, and G. Moser, Phys. Rev. E **85**, 021143 (2012).

[14] P. Calabrese, A. Pelissetto, and E. Vicari, Phys. Rev. B **67**, 054505 (2003).

[15] L. T. Adzhemyan, E. V. Ivanova, M. V. Kompaniets, A. Kudlis, and A. I. Sokolov, Nucl. Phys. B. **940**, 332 (2019).

[16] W. Selke, Phys. Rev. E **83**, 042102 (2011).

[17] S. H. Tsai, S. Hu, and D. P. Landau, J. Phys.: Conf. Ser. **487**, 012005 (2014).

[18] M. Henkel and M. Pleimling, *Non-equilibrium Phase Transitions*, Vol. 2 (Springer, Berlin, 2010).

[19] U. C. Täuber, *Critical Dynamics: A Field Theory Approach to Equilibrium and Non-equilibrium Scaling Behavior* (Cambridge University Press, Cambridge, UK, 2014).

[20] R. Nandi and U. C. Täuber, Phys. Rev. B **99**, 064417 (2019).

[21] R. Freedman and G. F. Mazenko, Phys. Rev. B **13**, 4967 (1976).

[22] R. Folk and G. Moser, J. Phys. A: Math. Gen. **39**, R207 (2006).

[23] S. Ma and G. F. Mazenko, Phys. Rev. Lett. **33**, 1383 (1974).

[24] K. Kawasaki, Phys. Rev. **145**, 224 (1966).

[25] R. J. Glauber, J. Math. Phys. **4**, 294 (1963).

[26] V. K. Akkineni and U. C. Täuber, Phys. Rev. E **69**, 036113 (2004).

[27] R. Folk and G. Moser, Phys. Rev. E **69**, 036101 (2004).

[28] M. Campostrini, M. Hasenbusch, A. Pelissetto, P. Rossi, and E. Vicari, Phys. Rev. B **65**, 144520 (2002).

[29] D. P. Landau, Physica A **205**, 41 (1994).

[30] K. Oerding and H. K. Janssen, J. Phys. A: Math. Gen. **26**, 3369 (1993).

[31] H. K. Janssen, B. Schaub, and B. Schmittmann, Z. Phys. B Condens. Matter **73**, 539 (1989).

[32] W. Koch and V. Dohm, Phys. Rev. E **58**, R1179(R) (1998).

[33] C. Sire, Phys. Rev. Lett. **93**, 130602 (2004).

[34] C. Godrèche, F. Krzakała, and F. Ricci-Tersenghi, J. Stat. Mech.: Theory Exp. (2004) P04007.

[35] B. I. Halperin, P. C. Hohenberg, and E. D. Siggia, Phys. Rev. B **13**, 1299 (1976).

[36] B. D. Josephson, Phys. Lett. **21**, 608 (1966).

[37] B. I. Halperin and P. C. Hohenberg, Phys. Rev. **188**, 898 (1969).

[38] K. Oerding and H. K. Janssen, J. Phys. A: Math. Gen. **26**, 5295 (1993).

[39] S. Chen and U. C. Täuber, Phys. Biol. **13**, 025005 (2016).

[40] J. D. Gunton and K. Kawasaki, Prog. Theor. Phys. **56**, 61 (1976).